Technical note

Modeling and machining evaluation of microstructure fabrication by fast tool servo-based diamond machining

Hong Lu [a], Deugwoo Lee [b,*], Jongman Kim [b], Soohyung Kim [b]

[a] Department of Nano Fusion Technology, Pusan National University, Miryang 627-706, South Korea
[b] Department of Nanomechatronics Engineering, Pusan National University, Miryang 627-706, South Korea

ARTICLE INFO

ABSTRACT

A fast-tool servo-machining process is typically utilized to generate sinusoidal microstructures for optical components only when the clearance angle of the cutting tool is greater than the critical value. This paper focuses on the generation characteristics of microstructures for surface texturing applications when the clearance angle of the cutting tool is smaller than this critical angle. A method for calculating the microstructure profile amplitude and wavelength is introduced for the prediction of microstructure generation. Cutting tests were conducted, and the measured results were quite close to the corresponding calculated results, further verifying the capability of the proposed analytical model.

Crown Copyright © 2013 Published by Elsevier Inc. All rights reserved.

1. Introduction

Ultraprecision microstructured surfaces with microscale or nanoscale resolution are fundamental for enhancing technical surfaces with specific functionalities, such as optical component usage [1], information storage [2], and tribological performance [3]. Optical and electronic methods for fabricating such microstructured surfaces include photolithography, electron beam writing, and focused ion beam machining. Although these methods are effective for fabricating three-dimensional microstructures with a regular configuration, they require a long fabrication period for large-area machining.

Fast-tool servo (FTS)-based diamond machining is an efficient process for producing micro- and nanostructured surfaces on a flat or cylindrical workpiece with a regular array of surface height features and specific functionality [4,5]. The working principle of FTS-based diamond turning on a cylindrical workpiece is shown in Fig. 1. A workpiece is clamped on the spindle; a tool servo is fixed on the slide of the machine and can move in the direction of the x-axis (feed rate direction). The cutting tool is translated in and out of the workpiece several times per revolution, in synchronization with the spindle rotation and x-axis slide, to obtain the microstructured surface. Depending on its bandwidth, the tool servo can be

regarded as a FTS or a slow tool servo (STS) [6]. However, no clear bandwidth boundary exists between them.

FTS-based diamond machining process is used widely for improving the form accuracy of the surface [7] or generating a functional surface on brittle material [8] or for optical components [9,10]. However, these studies only demonstrated the superiority of vibration machining when utilizing FTS to improve the surface form accuracy in ultraprecision manufacturing. Another application is the use of FTS to generate regular sinusoidal microstructures for optical components. Noh et al. [11] designed a voice coil motor (VCM)-assisted FTS to fabricate the micro-lens. Lu and Trumper [12] presented a spindle position estimation technique for effectively improving the form accuracy of one-dimensional (1D) and two-dimensional (2D) sinusoidal surfaces with a peak-to-valley amplitude of 2.041 μm. However, these studies did not discuss the FTS machining conditions in detail when the cutting tool clearance angle is smaller than its critical value.

This paper presents a modeling and manufacturing methodology for microstructures produced by FTS-based diamond machining in large-area surface texturing. The influence of cutting tool geometric parameters (such as clearance angle and nose angle) on microstructure generation is investigated. A method for calculating the microstructure profile amplitude and wavelength is introduced for the prediction of microstructure generation prior to the FTS machining process, especially when the clearance angle of the tool is smaller than the critical value. Finally, a series of cutting tests is carried out, and the experimental results are analyzed and compared with the corresponding calculated values.

* Corresponding author. Tel.: +82 55 350 5666; fax: +82 55 351 2982.
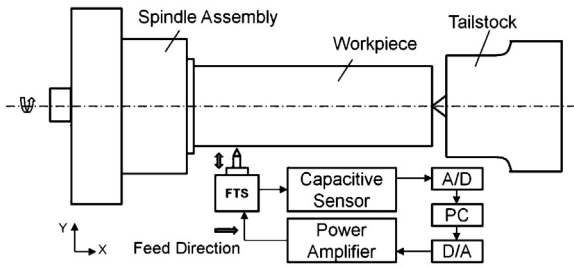E-mail addresses: hlu@pusan.ac.kr (H. Lu), dwoolee@pusan.ac.kr (D. Lee).

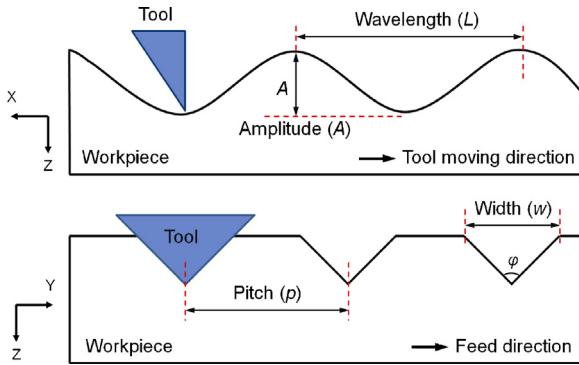**Fig. 1.** Working principle of FTS-based diamond turning on a cylindrical workpiece.

Fig. 2. Schematic diagram of microstructure generation.

2. Modeling of microstructure generation

Compared with conventional diamond machining, FTS-based diamond machining offers an indispensable solution for fabricating complicated microstructured surfaces, such as 1D and 2D sinusoidal surfaces [11] and a micro-lens array on a roller [12], without the need for any type of post-processing. A diagram of microstructure generation via FTS-based diamond machining is shown in Fig. 2.

The microstructure profile along the x-axis is generated by tool vibration, while the profile along the y-axis is generated by the shape of the tool. The pitch (p) between two grooves is determined by the feed rate of the cutting tool. The width (w) and angle (φ) of the groove is related to the amplitude of the profile (A) and the nose angle of the cutting tool (α). The wavelength (L) of the profile

(along the x-axis) depends mainly on the machining conditions and is given by the following equations:

$$L = V \cdot \frac{1}{f}, \quad \text{for the cutting} \tag{1}$$

$$L = \frac{n}{60} \cdot 2\pi r \cdot \frac{1}{f}, \quad \text{for the turning} \tag{2}$$

where f is the driving frequency of the FTS, V is the cutting speed, n is the spindle speed in rpms, and r is the radius of the workpiece being turned. Above all, the configuration of microstructures is mainly determined by the machining conditions and the shape of the cutting tool.

The tool geometry, which is mainly specified by the tool nose angle, clearance angle (θ), and rake angle, must be selected for a desired microstructure to guarantee form accuracy and microstructure profile generation along the y-axis (in the y–z-plane). FTS-based diamond machining has two primary applications. One is the generation of regular sinusoidal microstructures for optical components. In this application, the clearance angle of the cutting tool plays an important role in ensuring that the cutting process can proceed without interference between the microstructures and the cutting tool. If θ is not large enough, the machined microstructures will be flattened the next time the tool cuts into the bottom of groove, as shown in the shaded portion of Fig. 3(c). Depending on the designed dimensions of the microstructures, the desired value of θ can be calculated from the following equation:

$$\theta > \arctan\left(\frac{2A}{L}\right) \tag{3}$$

where A is the amplitude of the profile. Although this equation is an approximation and only provides an approximate value of θ, it is adequate for microstructure generation with L equal to several hundred micrometers.

For other applications, such as texturing a workpiece surface for improved tribological performance or producing a master roller for roll-to-roll processing, standardized sinusoidal structures are not required, but regular microstructure arrays with L smaller than 100 μm are needed. Hence, a small clearance angle is usually selected for large-area micromachining to ensure the tool lifetime.

Fig. 3 illustrates the generation analysis of a variety of microstructure profiles with increasing L and constant θ. The red line represents the flank edge of the cutting tool. The black solid line is the machined profile, and the black dotted line is the flattened part. The configuration bounded by the black solid line, and the red
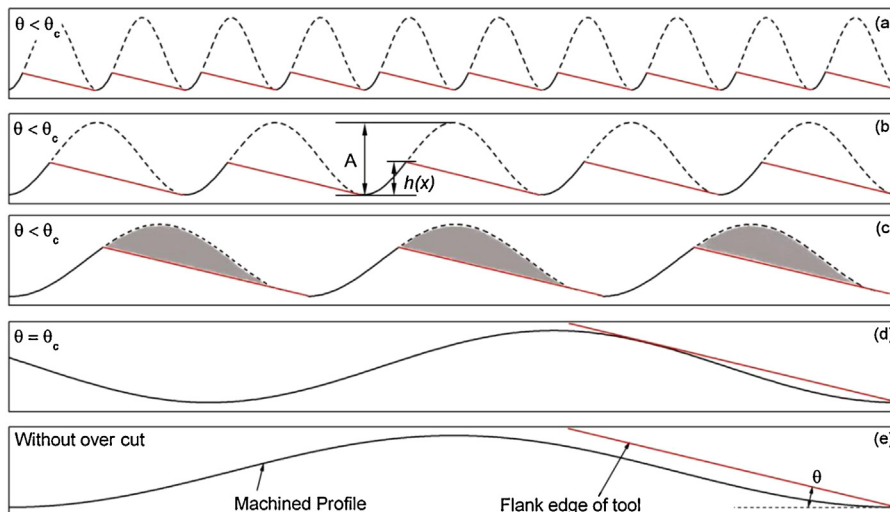

Fig. 3. Generation analysis of a variety of microstructure profiles with increasing L and constant θ.
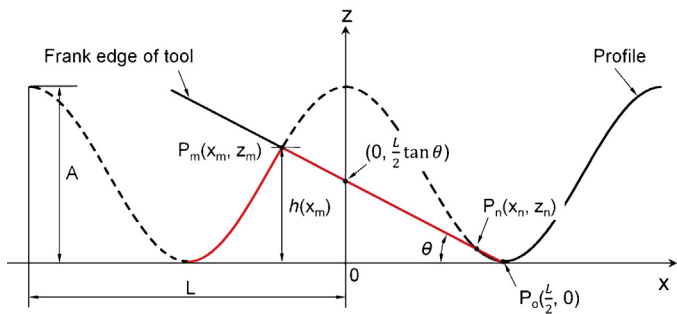
Fig. 4. Geometry for the calculation of the points of intersection between $h(x)$ and $l(x)$.

line is the actual microstructure profile when $\theta < \theta_c$, as shown in Fig. 3(a)–(c). Here θ_c is the critical value of θ, which only occurs when the tool tip just touches the valley of the profile, and the flank edge of the tool is tangent to the profile, as shown in Fig. 3(d). Fig. 3(e) shows the sinusoidal profile generation when $\theta > \theta_c$.

Fig. 4 provides a graph for computing the points of intersection between the wave equation of the profile $h(x)$ and the linear equation of the flank edge of the tool $l(x)$. A single wavelength has three points of intersection: P_m (x_m, z_m), P_n (x_n, z_n), and P_o $(L/2, 0)$. The z-coordinate $h(x_m)$ of P_m determines the actual amplitude of the profile. The horizontal axis represents the cutting direction, and the vertical axis is the z-axis. From the geometric relationship illustrated in Fig. 4, the following set of equations can be obtained:

$$
\begin{cases}
l(x) = \tan \theta \cdot \left(\dfrac{L}{2} - x \right) \\
h(x) = A \cos 2\pi \left(\dfrac{x}{L} - ft \right) + A
\end{cases}
\tag{4}
$$

where t is the time in seconds.

The points of intersection are calculated by solving this set of equations. By using the *Maclaurin series* to expand the cosine function, (4) can be simplified to the following:

$$
2A \left(\frac{\pi}{L} \right)^2 x^2 - \tan \theta \cdot x + \frac{L}{2} \tan \theta - 2A = 0
\tag{5}
$$

Eq. (5) provides a method for calculating the coordinates of the points of intersection between the wave equation of the profile and the linear equation of the flank edge of the tool. The desired profile amplitude can be modeled by this equation prior to FTS machining.
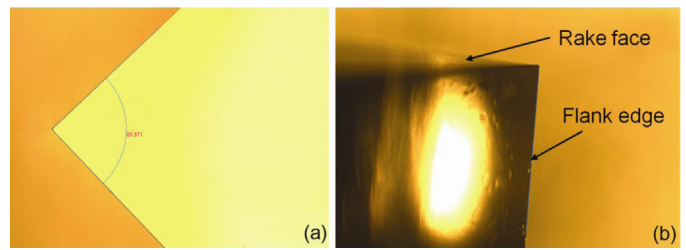

Fig. 6. Microscopic images of the diamond tool: (a) top view and (b) side view.
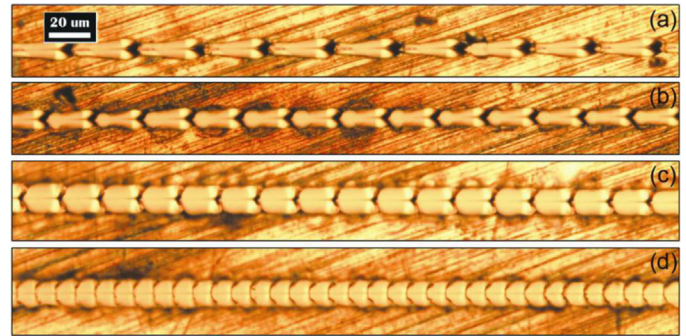

Fig. 7. Microscopic images of microstructures formed with the driving frequency of: (a) 30 Hz; (b) 40 Hz; (c) 50 Hz and (d) 100 Hz.

3. Experiments and discussion

To verify the proposed model, a copper-alloy specimen was machined on a precision lathe (UPL-200). The lathe consisted of x-, y-, and z-axes and a rotation table. The rotation table was mounted on an isolator to prevent external vibration, while maintaining high structural stiffness. The x-axis, controlled by an air guide and a linear motor with a 100-nm resolution, provided the cutting direction for the diamond tool. The y- and z-axes, controlled by linear guides equipped with a ball-screw and needle roller-bearing stepping motor with a 10-nm resolution, enabled accurate positioning for the machining. A specially designed piezoelectric actuator-assisted linear FTS was used for the microstructure fabrication. This FTS had a diamond tool fixed in the tool holder and was connected to the fixed body via two sets of parallel leaf springs (with a thickness of 1 mm). The piezoelectric actuator had a displacement of up to 120 μm, an axial stiffness of 20 N μm^{-1}, and a maximum driving
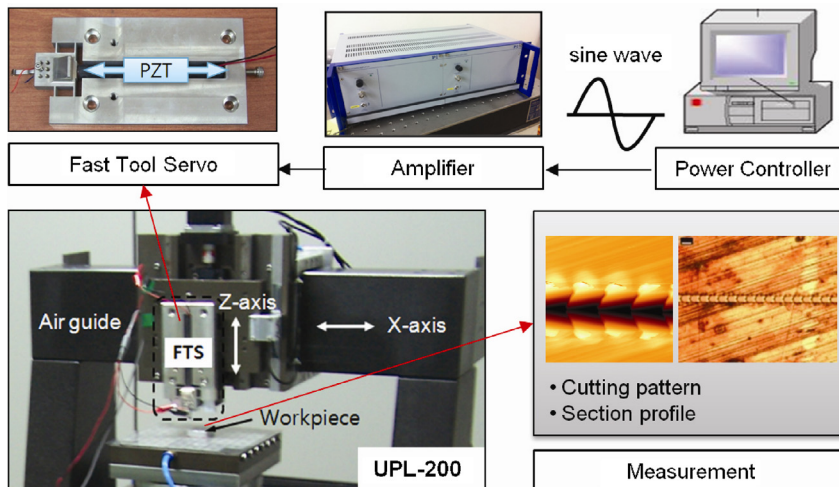

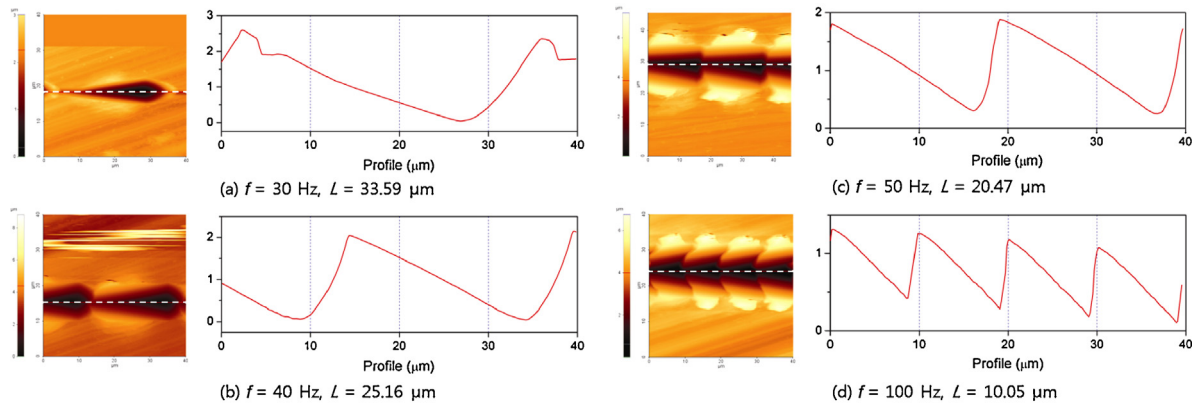**Fig. 5.** Machining test set up.

Fig. 8. AFM images and profiles of microstructures generated with different frequency.

force of 2400 N. A capacitive displacement sensor was used for position measurement, with a displacement signal range of −250 to +250 μm and resolution of 2.9 nm. The bandwidth of the capacitive displacement sensor was set at 5 kHz in response to the maximum frequency required for fast tracking performance of the FTS.

A PC equipped with the LabView software package was used to generate the input signals. These signals were output to a PI high voltage amplifier, and the amplified signals were then supplied to the piezoelectric actuator as the driving signals, as shown in Fig. 5. The machining conditions used in this investigation are listed in Table 1. The cutting tool was a single-crystal diamond tool with a nose angle of 90°, a nominal rake angle of 0°, and a clearance angle of 5°. Fig. 6 shows microscopic images of the diamond cutting tool used in the experiments.

The quality of the machined microstructure was evaluated by optical microscopy, scanning electron microscopy (SEM), and atomic force microscopy (AFM). Fig. 7 shows microscopic imagines from four cutting tests examined under low magnification. In the cases shown, the tool was driven by sinusoidal oscillations with a cutting speed of 60 mm min^{-1} and frequencies of 100, 50, 40, and 30 Hz (corresponding to Fig. 7(a)–(d), respectively). Each individual oscillation is clearly distinguishable in the images, and the microstructures are free of breakage. The machining parameters used for the workpiece in Fig. 7 were the result of several series of tests.

Fig. 8 shows AFM images of the copper-alloy specimens for evaluating the profile quality of the microstructures, which were machined at the same cutting speed and driving frequencies as the samples shown in Fig. 7. The profiles of four kinds of microstructures are shown, which positions are marked with dotted lines in the height maps on the left side of the figure. The measured results for the profile wavelengths were 10.05, 20.47, 25.16, and 33.59 μm, respectively, as shown in the graphs on the right side of Fig. 8(a)–(d). These results were quite close to the corresponding
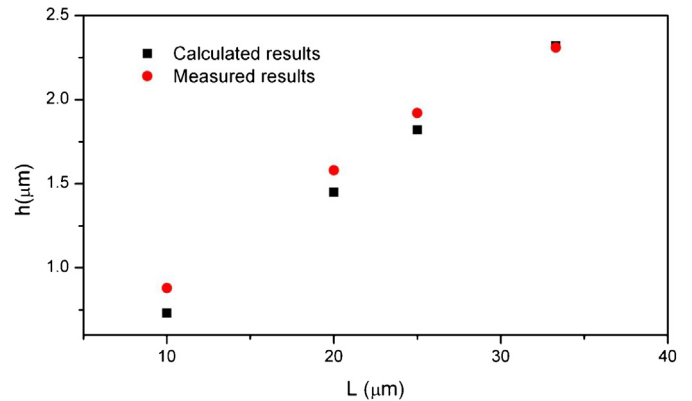

Fig. 9. Comparison of profile amplitude between different microstructures generated by same cutting tool.

calculated values, which were 10, 20, 25, and 33.3 μm, respectively (obtained via Eq. (1)).

The measured profile amplitude results and corresponding calculated results (obtained via Eq. (5)) are compared in Fig. 9, and the measured amplitudes and calculated values were in good agreement. The difference between them decreased with increasing profile wavelength, due to the reduction of the flattened materials. These results further verify the capability of the proposed analytical model for predicting microstructure generation by FTS-based diamond machining. Fig. 10 shows lateral SEM images of the microstructures produced with driving frequencies of 100, 40, and 10 Hz, respectively, using the same cutting tool and cutting speed of 60 mm min^{-1}. Burr formation and piling are clearly evident in Fig. 10(a) and (b). Burr formation diminished with increasing L due to the reduction of the flattened part during the machining
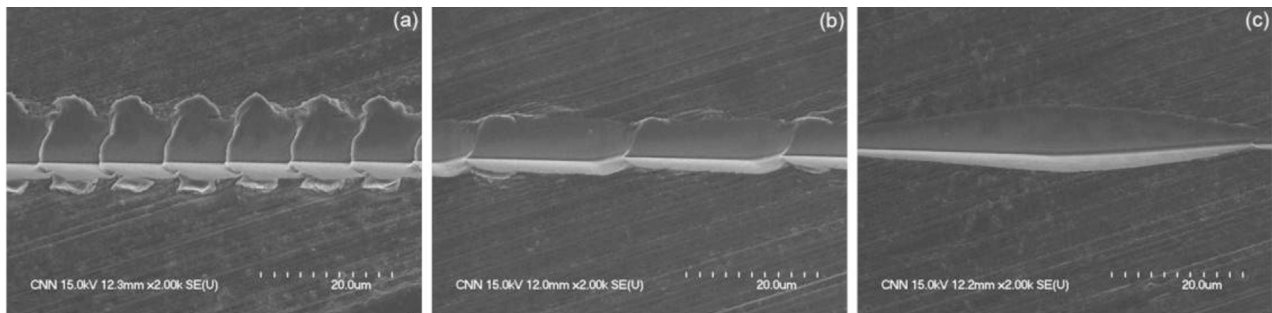

Fig. 10. SEM images of microstructures in tilted view generated with the driving frequency of: (a) 100 Hz; (b) 40 Hz; (c) 10 Hz.

Table 1
Machining conditions.

Workpiece material	Cutting depth [μm]	Driving frequency [Hz]	Cutting speed [mm min^{-1}]	Cutting distance [mm]
Copper alloy	4	10, 30, 40, 50, 100	60	20

process. The burrs disappeared altogether in Fig. 10(c), which shows a sinusoidal profile without any flattened materials.

4. Conclusions

Fast-tool servo-based diamond machining was effective for generating defined microstructures on a workpiece and can be used for surface texturing, especially when the clearance angle of the cutting tool is smaller than the critical angle. The machining tests indicate that a part of the fabricated sinusoidal structure was flattened by the flank edge of the cutting tool when the clearance angle is smaller than the critical value. Therefore, a particular microstructure will be generated in the groove. A method for calculating this microstructure profile amplitude and wavelength was introduced. The measured results from the cutting tests were quite close to the corresponding calculated results and further verify the capability of the proposed analytical model. The test results also show that reduction of the microstructure profile wavelength leads to increased burr formation at the edge of the groove due to the growth of the flattened materials during the machining process. How to diminish the formation of burrs will be investigated in future work.

Acknowledgements

References

[1] Scheiding S, Yi AY, Gebhardt A, Li L, Risse S, Eberhardt R, et al. Freeform manufacturing of a microoptical lens array on a steep curved substrate by use of a voice coil fast tool servo. Optics Express 2011;19(24):23938–51.

[2] Denkena B, Boehnke D, Spille C, Dragon R. In-process information storage on surfaces by turning operations. CIRP Annals-Manufacturing Technology 2008;57:85–8.

[3] Greco A, Martini A, Liu Y, Lin C, Wang QJ. Rolling contact fatigue performance of vibro-mechanical textured surfaces. Tribology Transactions 2010;53:610–20.

[4] Dow TA, Miller MH, Falter PJ. Application of a fast tool servo for diamond turning of nonrotationally symmetric surfaces. Precision Engineering 1991;13(4):243–50.

[5] Rakuff S, Cuttino JF. Design and testing of a long-range precision fast tool servo system for diamond turning. Precision Engineering 2009;33:18–25.

[6] Yi AY, Li L. Design and fabrication of a microlens array by use of a slow tool servo. Optics letters 2005;30(13):1707–9.

[7] Kong LB, Cheung CF. Modeling and characterization of surface generation in fast tool servo machining of microlens arrays. Computers and Industrial Engineering 2012;63:957–70.

[8] Yu DP, Wong YS, Hong GS. Ultraprecision machining of micro-structured functional surfaces on brittle materials. Journal of Micromechanics and Microengineering 2011;21:095011.

[9] Lu H, Lee DW, Lee SM, Park JW. Diamond machining of sinusoidal grid surface using fast tool servo system for fabrication of hydrophobic surface. Transactions of Nonferrous Metals Society of China 2012;22:s787–92.

[10] Lu H, Choi SC, Lee SM, Lee DW. Microstructure of fast tool servo machining on copper alloy. Transactions of Nonferrous Metals Society of China 2012;22:s820–4.

[11] Noh YJ, Nagashima M, Arai Y, Gao W. Fast positioning of cutting tool by a voice coil actuator for micro-lens fabrication. International Journal of Automation Technology 2009;3(3):257–62.

[12] Lu X, Trumper DL. Spindle rotary potion estimation for fast tool servo trajectory generation. International Journal of Machine Tools and Manufacture 2007;47:1362–7.